

Mechanical Properties of the Aortic Arch as a Function of Growth

A THESIS SUBMITTED TO THE FACULTY OF THE UNIVERSITY OF MINNESOTA

BY

Ross Daniel Hinrichsen

IN PARTIAL FULFILLMENT OF THE REQUIREMENTS FOR THE DEGREE OF
MASTER OF SCIENCE

Advisor: Dr. Paul Iaizzo

November 2016

Copyright

Ross Hinrichsen 2016

Acknowledgements

I would like to thank my advisor, Paul Iazzo, for his support through this project and access to the Visible Heart Lab's resources and knowledge. From the Visible Heart Lab I would like to specifically thank Charles Soule for his assistance with data collection and Erik Gaasedelen for helping me with data analysis techniques. Also, I would like to thank the rest of the students and faculty from the Visible Heart Lab for not rolling their eyes too hard when I asked dumb questions.

I would also like to thank Christopher Korencuk for guiding me through the strain tracking protocol from Victor Barocas' lab and his assistance troubleshooting the process.

Finally, I would like to thank Professors Victor Barocas and Patrick Alford for the original inspiration for my research and their guidance along the way.

Abstract

The aortic arch is defined as the portion of aorta that curves between the ascending and descending segments. Due to its varied geometry and thus differing applied forces during pulsatile blood flow, the thickness of the aorta varies due to muscle growth as modeled by Alford et al. The purpose of this study was to better assess the regional hyperelastic mechanical properties of the aorta, as well as its intrinsic contractility.

For the hyperelastic properties, axial strips of aortic arch taken from different anatomical positions were tested using a uniaxial pull tester. These tests showed a correlation between the circumferential position of the sample (Φ) and the hyperelastic properties. From the data, the material's shear modulus exhibited an average maximum difference of about 35%, with larger wall thicknesses leading to a decreased modulus.

For the circumferential properties, step-by-step strain tracking was required, as the thickness would vary across the strip. Testing was performed using the same machine, but samples were patterned with Verhoeff stain and filmed during the test. This assessment revealed the same relationship as the axial samples, with the modulus decreasing due to enhanced muscle thickness.

To determine the contractile effects of asymmetric anatomic aortic thicknesses, samples were cut into half-rings at points designed to give the largest possible difference in thickness. These rings were then subjected to a cycle of 1 μ M norepinephrine to induce contraction, followed by a neutral buffer for relaxation. The inner aortic half-rings displayed twice as much contractile force compared to the outer half-rings when normalized to wall thicknesses.

The decreased shear modulus and increased contractile properties uniquely observed in these experiments may indicate that much of the arterial anatomic specificity takes place within the tunica media; i.e. with recruitment of elastin fibers and smooth muscle cells.

Table of Contents

Contents

Acknowledgements.....	i
Abstract.....	ii
List of Tables.....	vi
List of Figures	vii
Introduction & Background	1
Anatomic and Physiological Features of the Aortic Arch	1
Geometry of the Aortic Arch	2
Boundary Conditions of the Aortic Arch.....	3
Aortic Wall Development and Remodeling.....	4
Associated Aortic Diseases and Medical Concerns	4
Experimental Equipment and Resources	6
Experimental Protocol	8
3.1: Uniaxial Sample Testing.....	8
3.2: Circumferential Sample Testing	10
3.3: Contractile Properties Protocol.....	11
Data Analyses.....	15
4.1: Axial Test Analysis	15
4.2 Circumferential Testing Analysis.....	22
4.3 Contractility Testing Analysis.....	23
Results	24
5.1 Uniaxial Testing	24
5.2 Circumferential Testing.....	31
5.3 Contractile Testing.....	34
Conclusions & Future Considerations.....	36
Bibliography	38
Appendix A: Matlab Code	39
Avulsion Force Determination.....	39
Neo-Hookian Curve Fitting.....	40
Mooney-Rivlin Curve Fitting	42

Yeoh Curve Fitting.....	44
Fung Curve Fitting	46
Strain Tracking Stretched Width Analysis.....	48

List of Tables

Table 1: Experimental Equipment.....	7
Table 2: Recipe for 4 Liters of Skeletal Krebs-Henseleit Solution.....	12
Table 3: Hyperelastic Model Equations	18
Table 4: Hyperelastic Model Equations as a Function of λ	19
Table 5: Shear Modulus Equations	20
Table 6: Neo-Hookian Shear Moduli.....	27
Table 7: Mooney-Rivlin Shear Moduli.....	27
Table 8: Yeoh Shear Moduli	28
Table 9: Fung Shear Moduli	28
Table 10: Contractile Test Results.....	34

List of Figures

Figure 1: Layers of elastic arteries, including the aortic arch	2
Figure 2: diagram of the human aortic arch with branching vessels.....	3
Figure 3: Stress concentration gradient in a half-torus	4
Figure 4: Pull tester and clamping system used in experiment	7
Figure 5: Cutting diagram for axial samples	8
Figure 6: Cutting diagram for circumferential samples	10
Figure 7: Muscle bath setup for contractile tests	14
Figure 8: Example of a nearly ideal test	15
Figure 9: Example of a test with large breakage before failure.....	16
Figure 10: Mesh overlaid on the testing sample	22
Figure 11: Plot of contractile force of samples over time due to buffer changes	23
Figure 12: Measured arterial wall thickness by circumferential position	24
Figure 13: Comparison of one uniaxial test to its calculated fits.....	25
Figure 14: Shear moduli calculated at $\lambda=1.4$ from four different models	26
Figure 15: Prediction of shear modulus from models as a function of circumferential position	29
Figure 16: Prediction of elastic modulus from models as a function of circumferential position	30
Figure 17: Average relative error of models at different stretch rates	31
Figure 18: Video capture, meshing, and strain results of circumferential strain tracking	32
Figure 19: Elastic Modulus vs circumferential position from strain tracking	33

Introduction & Background

Anatomic and Physiological Features of the Aortic Arch

The aortic arch, while differing in tortuosity/structure, has the same basic physiological makeup of ascending and descending aorta. This means it consists of the following major layers:

- Tunica adventitia: Consists of fibroblasts, bundles of collagen fibers, and a loose network of elastic fibers. It is relatively thin compared to the tunica media.
- Tunica media: Consists of alternating layers of elastin and smooth muscle cells with an extracellular matrix of collagen and elastin. It is the thickest layer of the elastic artery.
- Tunica intima: Consists of the endothelium and elastic interna. The endothelium is the inner lining for the vessel, providing a smooth wall that allows selective diffusion between the blood and vessel wall ¹

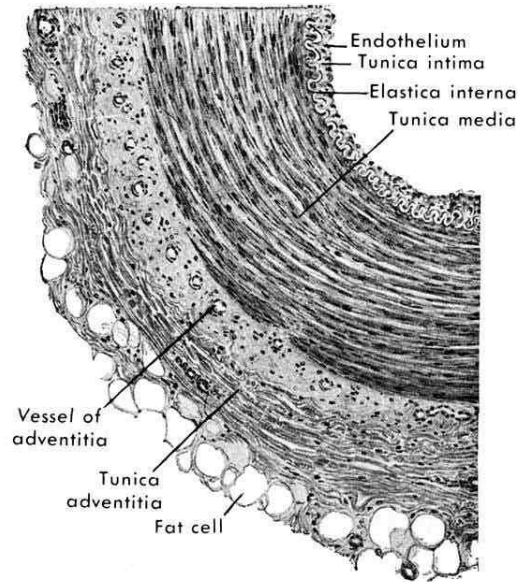


Figure 1: Layers of elastic arteries, including the aortic arch¹

Geometry of the Aortic Arch

The general anatomic appearance of the aortic arch is roughly equivalent to a half torus, as it connects the ascending and descending aorta. In humans, there are typically three primary branching vessels that arise on the top of the arch; these consist of the brachiocephalic artery, left carotid artery, and left subclavian artery. For porcine arches, which were investigated in this study, there are only two branching vessels: the right and left brachiocephalic trunk. Note, both of these vessels branch within a few centimeters, then primarily branch into subclavian and common carotid arteries²

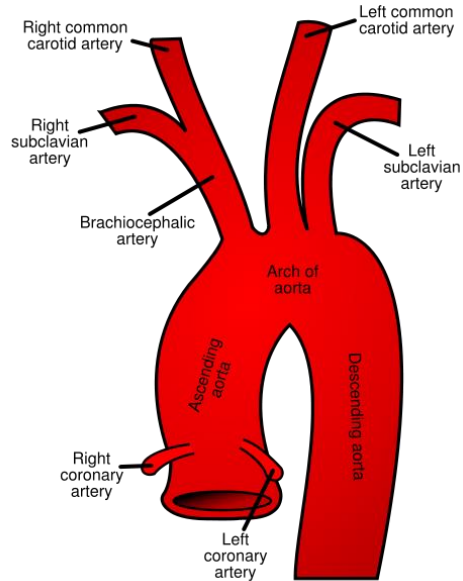


Figure 2: diagram of the human aortic arch with branching vessels. Porcine arches have one less vessel originating from the main branch.²

Boundary Conditions of the Aortic Arch

Due to its proximity to the aortic valve and the left ventricle, the aortic arch is exposed to constant fluctuation of pressures. In humans, a healthy systolic/diastolic pressure is normally determined to be 120/80 (mmHg) or below. However, hypertension can raise this to over 160/100 with dangerous effects. Note, that in some clinical cases and with extreme stress and exercise systolic pressures can exceed over 200 mmHg.³ Porcine hearts such as those tested can elicit similar pressures as to normal human hearts.⁴

Aortic Wall Development and Remodeling

Muscle growth occurs as a response to stress, i.e., typically recruiting more muscle cells to maintain geometry. In the aortic arch, the torus shape and resulting flow patterns during heart function results in a stress concentration in the inner aortic curvature. Over time this increased stress results in a thicker wall at the location of these gradients. It has been proposed that elastin is responsible for the growth regulation due to its low turnover rate.⁵

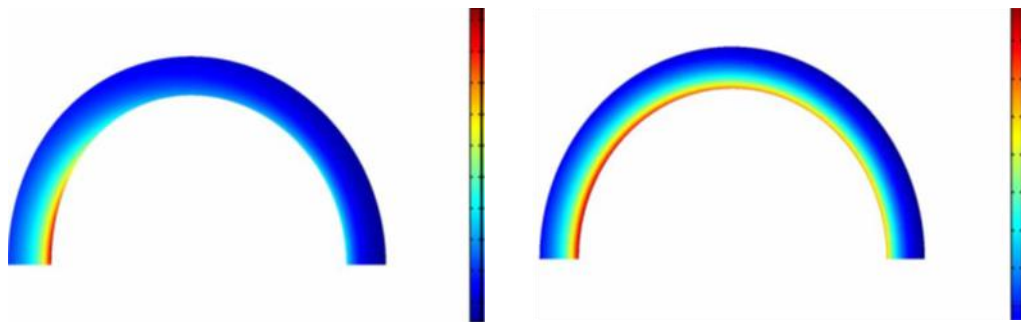


Figure 3: Stress concentration gradient in a half-torus. The inner curvature experiences the largest Cauchy stress, resulting in increased muscle growth⁵

Associated Aortic Diseases and Medical Concerns

It is considered that proper modeling of a given patient's aorta would be beneficial to the predication and treatment of life-threatening conditions. For example, an aortic aneurysm, a bulge within the aorta, affects over three million Americans per year. These bulges will continue to weaken the structures of the wall, as the increased loads prevent normal elastic function. The human body's mechanical response can also be compromised by plaque buildup, or atherosclerosis, reducing the artery's ability to expand. This can lead to conditions such as arteriosclerosis or coronary heart disease.⁶

If the whole cardiovascular system, beyond the aorta, could also be modeled more effectively, including vessel mechanics and fluid flow, it would be possible to predict and prevent these occurrences with greater accuracy.

Experimental Equipment and Resources

Aortic samples were taken from 5-8 month old Yorkshire-cross swine. These samples were sourced either from the University's Visible Heart Lab or the Meat Science Laboratory (Andrew Boss).

One problem to consider for these investigations was how samples were attached to the testing apparatus. Previous experiments had sutured loops at each end of the dogbone, which were then attached to the force tester. This potentially created two problems: 1) the suture would often slip off the sample, and 2) the loops created a natural breaking point by tightening on the sample. It was observed that this slippage could be mitigated by applying a small amount of superglue to the sutures on the sample. Yet, often it was difficult to gauge the amount of glue needed and/or the required drying times: i.e., as samples left exposed too long would begin to stiffen. Importantly, these problems were solved by designing a new attachment system for samples.

Specimen clamps were machined out of aluminum, using threaded bolts and bicycle wheel quick releases to provide an even pressure and reduce the likelihood of creating a weak point in the sample. The aluminum blocks were coated with 3M Safety Tape, which increased the surface friction to provide a better hold on the specimen. The top clamp was threaded onto the pull tester's load cell, while the bottom was held firmly in place with a vise connected to the base.

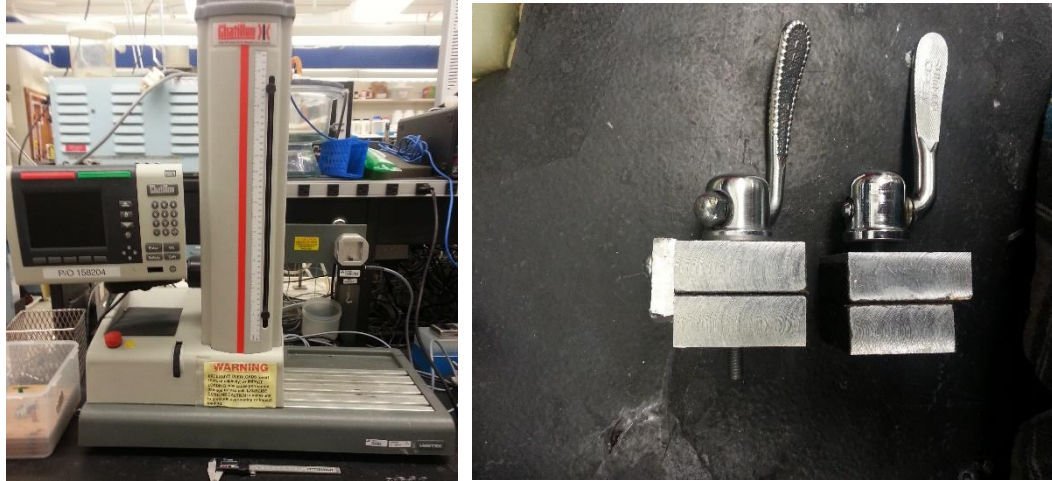


Figure 4: Pull tester and clamping system used in experiment

Table 1: Experimental Equipment

Equipment	Purpose	Accuracy/Specifications
Chatillon TCD 110, 50N Load Cell ⁷	Pull Testing	0.1% Accuracy, 1000Hz
Pittsburgh Digital Caliper	Linear Measurements	+/- 0.005 mm
Olympus PenLite EPL3 ⁸	Video Recording	1080p video, 30 fps
Grass FT03 Load Cell ⁹	Contractile Force Testing	1% Accuracy
Epilog Fusion Laser Cutter ¹⁰	Sample Cutting	1200 dpi

Experimental Protocol

3.1: Uniaxial Sample Testing

To assess the mechanical characteristics as a function of radial position on the aortic arch, axial strips were taken at 8 regular intervals (every 45°).

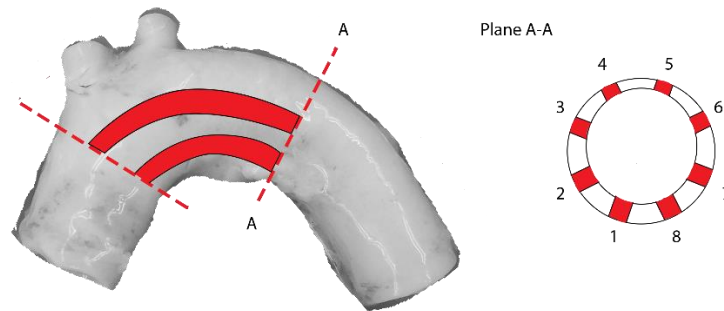


Figure 5: Cutting diagram for axial samples

This method allows the testing of elastic properties with a uniaxial tester while keeping the sample's thickness as consistent as possible. By measuring the thickness, width, and starting length of each sample a stress-strain relationship can be developed. A full arch could provide up to three sections of samples. However, the second section of each aorta was unable to provide 8 total samples due to branching arteries. The samples from the inner curvature could still be used.

- 1) Aortic arches were divided into three sections. Fatty tissue was removed from the aorta. Each section was then cut open to create a flat surface.
- 2) As described in the previous section, 8 samples were cut in each section of aorta arch using the laser cutter. If the samples did not separate completely on their own (due to excess moisture or fatty tissue), the incision was completed via scalpel. This maintained the dimensions created by the laser cutting pattern.
- 3) To set up the testing station, a 50N load cell was attached to the Chatillon TC110. The specialized clamps were then installed to hold specimens during testing. The top clamp was threaded onto the end of the load cell, while the bottom was held firmly in place via a vise attached to the base of the pull tester.
- 4) Prior to being tested, each strip was removed from the saline solution and measured with digital calipers to determine its width and depth.
- 5) The sample was then secured between the top and bottom clamps, with the narrow section of the dogbone shape exposed. The distance between the clamps' inner surface was recorded as the original length for calculation purposes. Each measurement (width, depth, length) was recorded in a lab notebook along with the arch number, section number, radial position (Φ), and testing time. These points were later transcribed to an Excel workbook for analysis.
- 6) Distance and force on the cell were zeroed out before commencing testing
- 7) For testing, the machine steadily separated the clamps at a rate of 1 mm/s while recording force output from the load cell. The test concluded when the sample failed. The data (load vs distance) was exported to a tsv file.
- 8) The pieces of the sample were discarded according to lab protocol

Steps 4-8 were repeated for each specimen

3.2: Circumferential Sample Testing

For circumferential properties, a different process was needed. Since aortic thickness varies around the circumference, strains needed to be tracked at different points within the sample. To achieve this, a circumferential strip was taken with a consistent width, and cut at 90° from the outer curvature of the arch to ensure that both the thickest and thinnest portions were being tested. The circumferential samples were also tested with a uniaxial machine, however with video being recorded of the test to analyze according to the protocol developed by Victor Barocas' lab, which will be discussed in Results and Analysis.

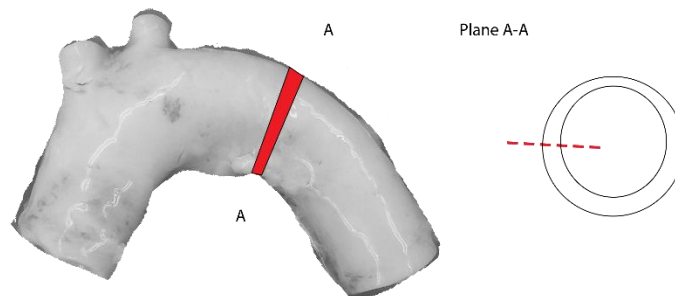


Figure 6: Cutting diagram for circumferential samples

The actual pull testing of circumferential strips was conducted identically to the axial strip tests. This includes the equipment used, rate pulled, and dimensional measuring. The difference comes in the preparation of samples and monitoring of the test itself.

- 1) Instead of near the inner curvature, the aortic arch was split along a line approximately 90° from the outer curvature. This was to ensure that both the thickest and thinnest portions of the artery were within the testing range of the dogbone.
- 2) Strips were laser cut in the same pattern as axial strips, but in the circumferential direction. They were also create singularly and in longer dogbones to encapsulate as much of the circumference as possible.
- 3) Each specimen was dusted on one side with powdered Verhoeff stain, attempting to get enough coverage to track strain without completely discoloring the specimen.
- 4) Setup of the pull tester is identical to the axial tests.
- 5) Before testing began, a GoPro Hero 4 was set up to take a video recording of the sample as it was stretched, with the stained side facing the camera.
- 6) For each test, the GoPro started recording before the pull tester was activated. Once the sample failed, the pull test was terminated and recording stopped. The tsv file of load vs distance was also collected from the pull tester.

3.3: Contractile Properties Protocol

In addition to the mechanical response of the aorta to stimulus, this study also aimed to briefly explore if relative growth of the aortic arch has any identifiable effects on its contractility. To test this, aortic rings were split at 90° and 270° , to give the largest difference between thicknesses. These were then attached to a load cell within a muscle

bath, suspended in a Krebs-Henseleit solution according to the following formula, which is scaled to make 4 liters of solution:

Table 2: Recipe for 4 Liters of Skeletal Krebs-Henseleit Solution

Ingredient	Amount (g)
Sodium Chloride (NaCl)	26.6072
Potassium Chloride (KCl)	1.014
Magnesium Sulfide (MgSO ₄)	0.9859
Glucose (C ₆ H ₁₂ O ₆)	7.992
Sodium Bicarbonate (NaCO ₃)	8.4008
Calcium Chloride (CaCl ₂)	1.4704

Ingredients were added in the order listed in Table 1. Before the calcium chloride was added, carbogen was added to the solution via a diffusion stone. This raised the pH of the solution slightly to avoid precipitation. This buffer was alternated with another solution of the same recipe, but with 1 μ M Norepinephrine to cause contraction of the endothelial cell layer. The resulting contractile forces were taken as analyzed in the context that different aortic thicknesses would elicit differences in induced contractions.

Due to the more time-sensitive nature of these tests, only porcine samples from the Visible Heart Lab experiments were used, as the time of death of the animal was known and the tests could be performed as soon as possible thereafter.

- 1) Clean muscle baths were filled with Krebs-Henseleit solution. Baths were maintained at 37 C
- 2) To determine if there was any physiological contraction in the aorta to measure, 8 total rings were cut: 4 from straight descending aorta and 4 from the aortic arch. All were cut at a ring width of 2-3 mm. These rings were then positioned inside a muscle bath via suture loops – one on the load cell, and another on a stabilizing hook underneath.
- 3) Each load cell was calibrated to read 2 g of force as a baseline and let rest for approximately 10 minutes to ensure the readings remained steady.
- 4) 1 liter of 1 μ M norepinephrine in Krebs-Henseleit was created. Once the baseline was set, the muscle baths were drained and replaced with the norepinephrine buffer. After the buffer change, the samples were left undisturbed for a period of approximately 45 minutes to allow elicitation of full contractions.
- 5) After 45 minutes and ensuring the load cell readings were remaining constant, the buffer was changed back to Krebs-Henseleit (with no norepinephrine) to induce relaxation. This was given the same window of 45 minutes to ensure a steady state.
- 6) Steps 4 and 5 were repeated with the same samples to see how the repeated cycles and added time affected results.
- 7) Each sample was removed from the buffer solution and its dried weight was recorded.



Figure 7: Muscle bath setup for contractile tests

Data Analyses

4.1: Axial Test Analysis

A total of 156 uniaxial tests on aortic arch samples were included in these analyses. Additionally, 16 tests using the same protocol were conducted on straight aorta as a form of population testing for verification. The tests showed a nonlinear elastic relationship between force and distance, as demonstrated in Figure 8

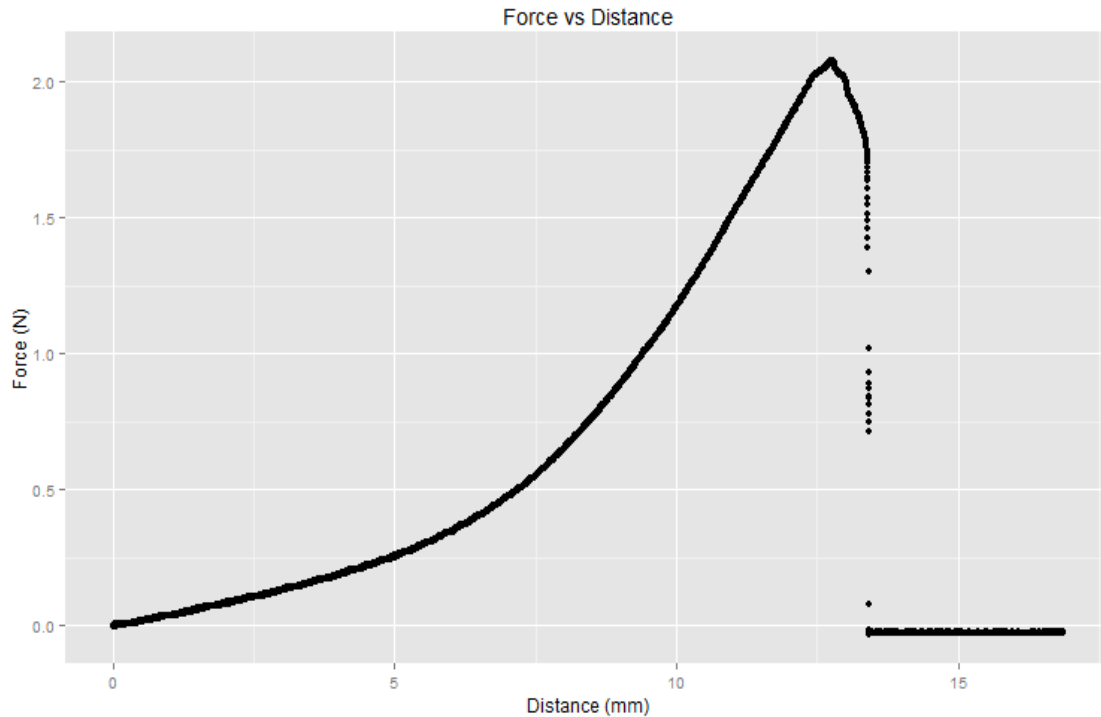


Figure 8: Example of a nearly ideal test, with no appreciable breakage before total failure

While Figure 8 shows a fairly ideal test, many of the samples had an extended period of breakage before complete failure, as demonstrated in Figure 9

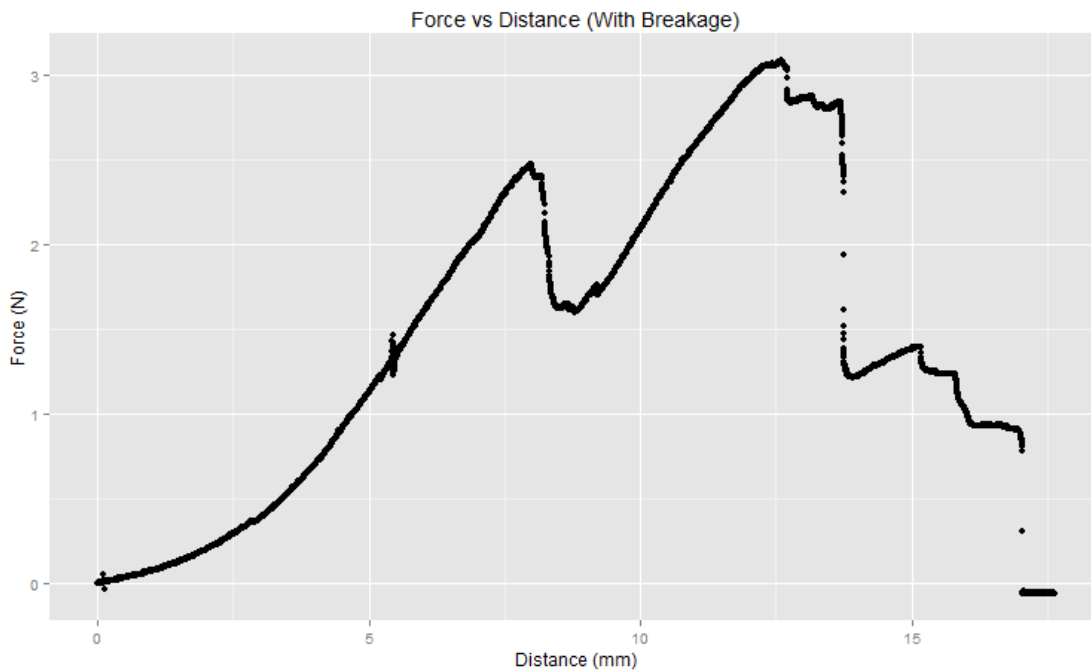


Figure 9: Example of a test with large breakage before failure. This makes stress calculations impossible, as the cross-sectional area is now unknown

The difficulty in analyzing these tests lies with predicting a given sample's relative cross-sectional area. While the changing area could be predicted during the beginning portion of the tests, there was no accurate way to model it afterward. To eliminate this uncertainty, all curve fitting was only conducted up until the avulsion force for each pull-test.

To analyze the results, the material was assumed to be incompressible and isotropic.⁵ This had the benefit of simplifying both the strain energy density models and area calculations throughout the test.

The stretch ratio, λ , was calculated at each point during the test according to

$$\lambda = \frac{(d + L_0)}{L_0} \quad (1)$$

Where d is the distance pulled (mm) and L_0 is the original length of the sample (mm)

Since incompressibility is assumed, the following relationship can be stated:

$$\lambda_1 \lambda_2 \lambda_3 = 1, \quad (2)$$

$$\lambda_2 = \lambda_3 = \frac{1}{\sqrt{\lambda}} \quad (\lambda_1 = \lambda) \quad (3)$$

Where λ is the principle stretch in each direction. In this analysis, λ_1 is the direction of the uniaxial stretch and will be referred to as λ . This allows prediction of how the cross-sectional area changes based on the change in λ

$$A = w * h \quad (4)$$

$$A = \lambda_2 w_0 * \lambda_3 h_0 = \frac{1}{\lambda} (w_0 * h_0) \quad (5)$$

Where w_0 and h_0 are the original width and thickness, respectively. The strain energy density was then calculated as

$$W = \frac{1}{2} \sigma \varepsilon \quad (6)$$

Where σ is the engineering stress and ε is the engineering strain. Curve fitting was performed using strain energy and stretch ratio (W vs λ).

The material assumptions also allow the calculation of the first and second invariants in each hyperelastic model based on just the stretch ratio in the tested direction.

$$I_1 = \lambda_1^2 + \lambda_2^2 + \lambda_3^2 = \lambda^2 + \frac{2}{\lambda} \quad (7)$$

$$I_2 = \lambda_1^2 \lambda_2^2 + \lambda_1^2 \lambda_3^2 + \lambda_2^2 \lambda_3^2 = 2\lambda + \frac{1}{\lambda^2} \quad (8)$$

Four hyperelastic models were fitted to the data, as shown in Table 2:

Table 3: Hyperelastic Model Equations

Model	Strain Energy Equation	Constant parameters
Neo-Hookian	$W = \frac{c}{2} (I_1 - 3)$	C
Mooney-Rivlin	$W = \frac{c_1}{2} (I_1 - 3) + \frac{c_2}{2} (I_2 - 3)$	C ₁ , C ₂
Yeoh	$W = A(I_1 - 3) + B(I_1 - 3)^2 +$	A, B, C

	$C(I_1 - 3)^3$	
Fung	$W = C * \frac{a*(I_1-3)+e^{a*(I_1-3)}-1}{2a}$	C, a

Table 3 shows the models when the stretch ratio is substituted for the invariants:

Table 4: Hyperelastic Model Equations as a Function of λ

Model	Strain Energy Equation
Neo-Hookian	$W = \frac{C}{2} (\lambda^2 + \frac{2}{\lambda} - 3)$
Mooney-Rivlin	$W = \frac{C_1}{2} (\lambda^2 + \frac{2}{\lambda} - 3) + \frac{C_2}{2} (2\lambda + \frac{1}{\lambda^2} - 3)$
Yeoh	$W = A (\lambda^2 + \frac{2}{\lambda} - 3) + B (\lambda^2 + \frac{2}{\lambda} - 3)^2 + C (\lambda^2 + \frac{2}{\lambda} - 3)^3$
Fung	$W = C * \frac{a*(\lambda^2+\frac{2}{\lambda}-3)+e^{a*(\lambda^2+\frac{2}{\lambda}-3)}-1}{2a}$

The shear modulus can be derived from these equations using¹¹

$$\mu(a) = \bar{\beta}_1 + \left(\frac{\bar{\beta}_{-1}}{\lambda} \right)$$

(9)

$$\bar{\beta}_1 = 2 * \frac{\partial W}{\partial I_1}, \quad \bar{\beta}_{-1} = 2 * \frac{\partial W}{\partial I_2}$$

Where μ is the shear modulus. Table 4 shows the shear modulus as calculated by each model:

Table 5: Shear Modulus Equations

Model	Shear Modulus
Neo-Hookian	$\mu = C$
Mooney-Rivlin	$\mu = C_1 - \frac{C_2}{\lambda}$
Yeoh	$\mu = 2 * \left(A + 2B \left(\lambda^2 + \frac{2}{\lambda} - 3 \right) + 3C \left(\lambda^2 + \frac{2}{\lambda} - 3 \right)^2 \right)$
Fung	$\mu = C * \frac{\alpha * \left(\lambda^2 + \frac{2}{\lambda} - 3 \right) + \exp \left(\alpha \left(\lambda^2 + \frac{2}{\lambda} - 3 \right) \right) - 1}{2\alpha}$

The Neo-Hookian model has a constant shear modulus across all stretch ratios. All others have an adjusted modulus as stretch increases.

The relative error for each test was also calculated at stretch ratios of $\lambda=1.1$ to $\lambda=1.6$ at increments of 0.1 according to

$$E = \left(\frac{W_{model}}{W_{actual}} \right) - 1 \quad (10)$$

If a test did not reach a calculated stretch before breaking, the error returned as exactly 1 and was discarded.

The Matlab code for each model can be found in Appendix A. Before curve fitting, the avulsion force was determined using the “Breakage” script, which takes user input to provide an end point for each test.

The fitting scripts were then run (one for each model). The script imported measured sample width, thickness, and length from each test along with the results from the “Breakage” script. The stretch ratio and strain energy were calculated using Equations 1 and 6, with Equation 4 providing the cross-sectional area.

Matlab’s “fitype” function was then run using the Levenburg-Marquardt method. Once the parameters from this had been obtained, it calculated the fit at $1.1 < \lambda < 1.6$ in increments of 0.1. If a test had failed before 1.6, those points returned an error of exactly 100% and were then discounted.

This process was run for each test, outputting the model parameters, R^2 value, and relative errors. These were collated in Excel and the shear modulus was calculated according to the equations in Table 4.

The elastic modulus was then calculated from the shear modulus using Equation 11.

$$E = \frac{\mu}{\lambda} * \left(\lambda^2 + \frac{2}{\lambda} \right) \quad (11)$$

With E as the elastic modulus. As $\lambda \rightarrow 1$, $E \rightarrow 3\mu$.

Statistical outliers were determined using Chauvenet's Criterion, with a maximum value chosen based on the sample size:

$$\tau = \frac{x - \bar{x}}{\sigma} < 2.2 \quad (12)$$

Any tests that exceeded the maximum value were omitted from results.

4.2 Circumferential Testing Analysis

For the mesh analysis, still frames of the video were taken at about 15 second intervals. This prevented any large strain jumps that may have made tracking difficult. Each frame was then cropped to eliminate as much of the background as possible, then converted to grayscale to improve contrast.

Abaqus was used to create the nodes for the mesh. Along each end, at least three points were selected and set to form a rigid line. The sample between these lines was outlined with nodes, which were then used to create a tetrahedral mesh. The coordinates of two distinct points were recorded in both the image and Abaqus to ensure the mesh was aligning correctly with the sample as it stretched.

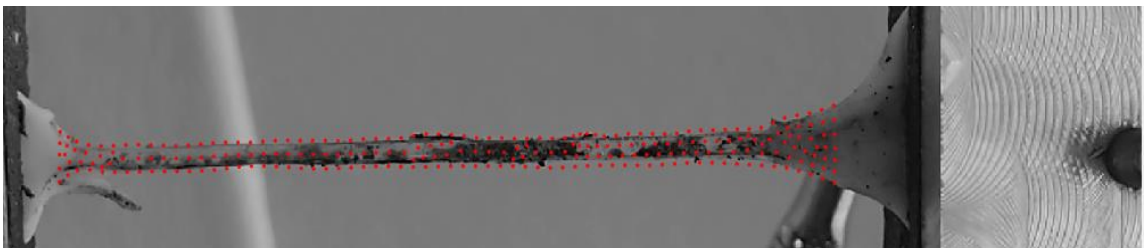


Figure 10: Mesh overlaid on the testing sample

This mesh was then analyzed according to the code developed by Victor Barocas' lab. It tracks the movement of each node throughout the test, allowing analysis of its movement relative to the rest of the mesh. The results are then displayed using tecplot 360, as shown in the Results section. The cross-sectional area can be calculated during stretch using the same formulae as the uniaxial testing, which can be used with the force and strain to calculate the elastic modulus

4.3 Contractility Testing Analysis

For the contractility tests, analysis was much simpler. Since the tests were over a long time period to allow the samples to settle, the important data points are directly before a buffer change. These changes are clear in the data, as seen in Figure 11.

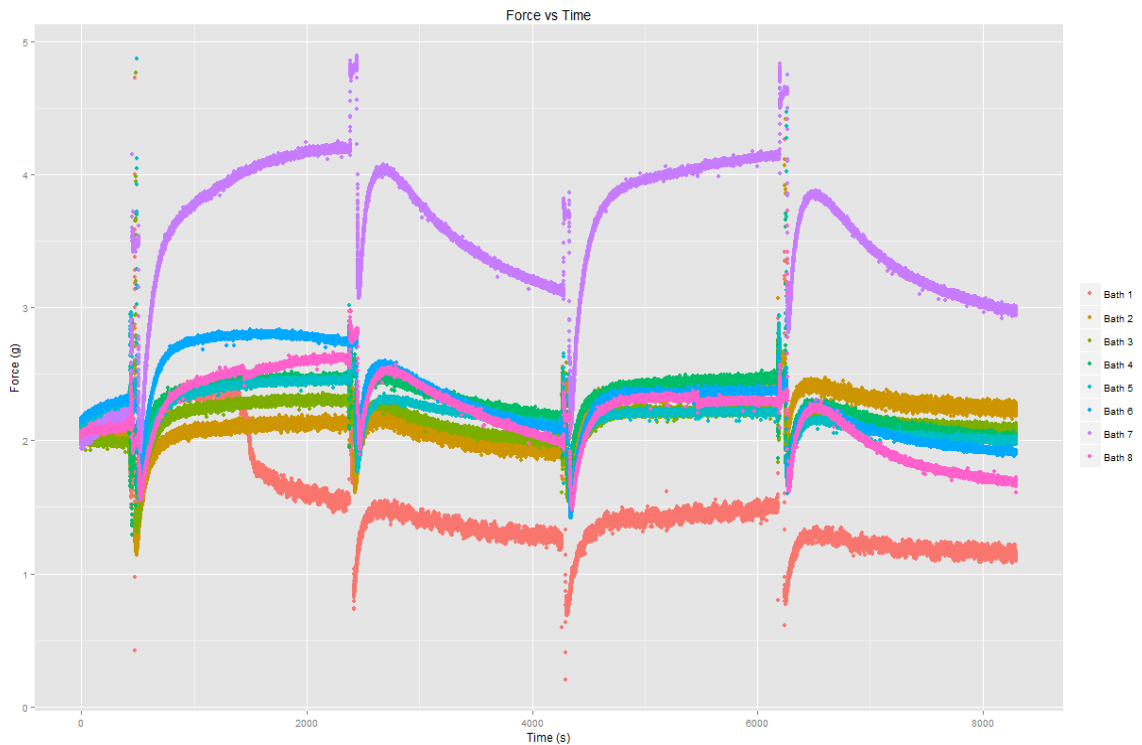


Figure 11: Plot of contractile force of samples over time due to buffer changes, set to an initial force of 2g.

The differences between forces at the end of each cycle were recorded and compared to see if there was a relation between contractility and wall growth.

Results

5.1 Uniaxial Testing

The relationship between radial position and thickness proposed in Alford et al was demonstrated by the gathered data

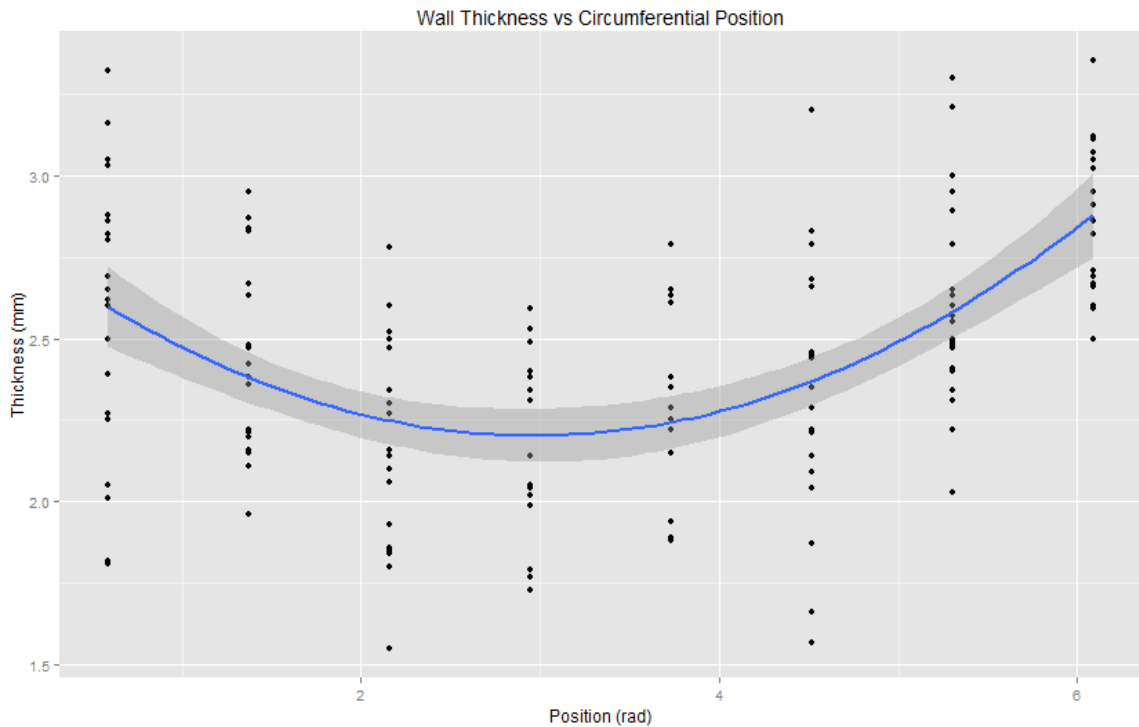


Figure 12: Measured arterial wall thickness by circumferential position

Figure 13 displays a sample test with all four models overlaid

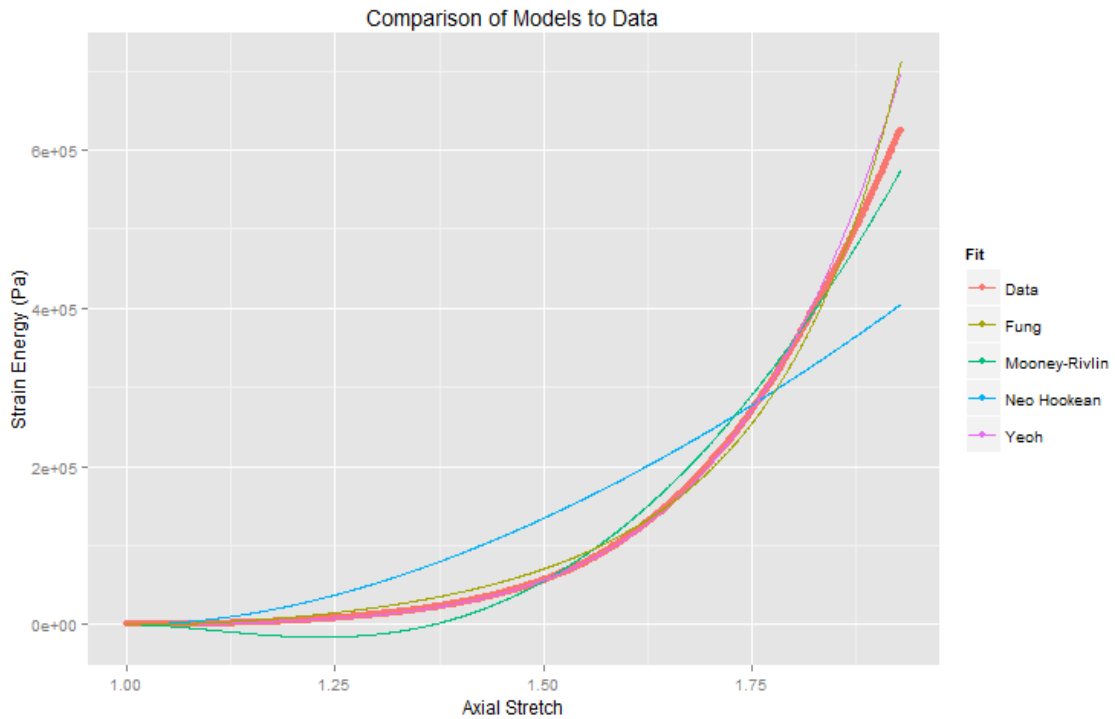


Figure 13: Comparison of one uniaxial test to its calculated fits

Curve fitting was very successful for most models. The Neo-Hookean model was the least accurate due to not accounting for a changing modulus, and had an average R^2 value of 0.8889. All other models had an average value of $R^2 > 0.99$.

For comparison, the calculated shear moduli as a function of radial position are presented in Figure 14. These are the values at $\lambda = 1.4$. This point was chosen due to the Neo-Hookean model's shear modulus being close to the other models. This allows comparison of the moduli more easily. The average modulus at each point is also shown, with a second-degree polynomial fit.

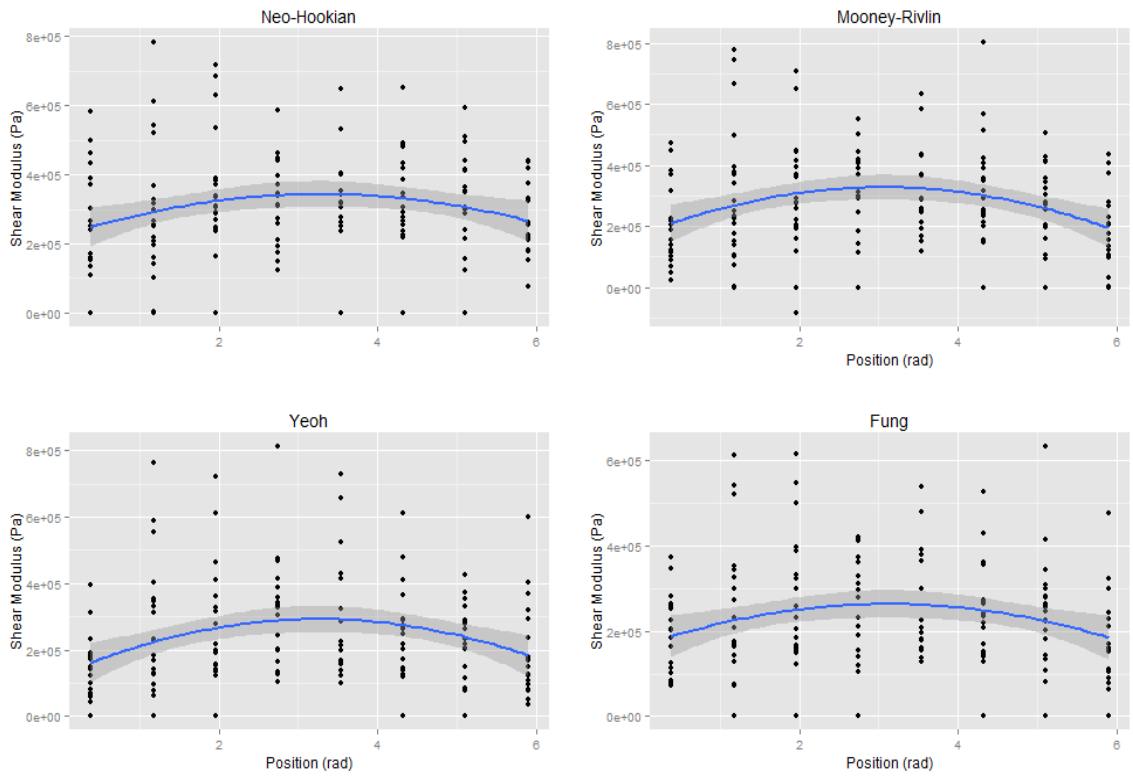


Figure 14: Shear moduli calculated at $\lambda=1.4$ from four different models

The numerical values for these averages as well as the standard deviation is shown in Table 5 to Table 8

Table 6: Neo-Hookian Shear Moduli

Φ	Rad	average μ	σ	average E	σ
1	0.392699	276280.84	145335.5	1044285.869	513446.7
2	1.570796	311065.64	180723	1275225.46	758137.3
3	2.356194	384246.43	163969.4	1449054.188	603992.1
4	3.141593	320356.54	126150.3	1186049.455	467043.6
5	3.926991	364273.31	113598.5	1310727.053	433693.7
6	4.712389	355474.16	119069.2	1360856.744	473526.7
7	5.497787	324373.21	123085.4	1305844.39	556872.9
8	6.283185	270501.68	106989.5	1294120.602	396105.2

Table 7: Mooney-Rivlin Shear Moduli

Φ	Rad	average μ	σ	average E	σ
1	0.392699	200415.68	133175.6	741994.881	493053.2
2	1.570796	314857.86	218826	1112705.84	828771.2
3	2.356194	311008.92	182741.1	1041780.82	729323.8
4	3.141593	341116.06	121733.7	1192745.53	528944.6
5	3.926991	312352.79	148996.9	1156417.34	551628.2
6	4.712389	337423.23	159886.6	1186773.37	640301.6
7	5.497787	313840.38	142571.2	1106595.08	573560.5
8	6.283185	195784.29	125052.1	684578.833	480550.7

Table 8: Yeoh Shear Moduli

Φ	Rad	average μ	σ	average E	σ
1	0.392699	148796.83	80982.23	495798.7026	330423.3
2	1.570796	259873.35	198357.4	874657.9834	753716.8
3	2.356194	293466.87	168394.6	931282.6404	694373.9
4	3.141593	311778.01	170610.9	1154289.34	631649.3
5	3.926991	302776	194547.5	1120961.408	720269.3
6	4.712389	264798.39	129223.1	931339.8022	514678.8
7	5.497787	253643.33	98230.49	849624.3787	445891.7
8	6.283185	199478.08	147251.8	738523.6049	545167.4

Table 9: Fung Shear Moduli

Φ	Rad	average μ	σ	average E	σ
1	0.392699	187928.95	93679.08	695765.5	346826.2
2	1.570796	246533.91	163940.8	829761.3	636739.9
3	2.356194	284421.81	145696.8	952722.5	601822
4	3.141593	268326.85	107420.9	938231	451320.5
5	3.926991	259487.13	131779.6	960693.9	487884.8
6	4.712389	251392.81	105193.6	884190.1	432441.4
7	5.497787	257034.78	119707.6	906299.6	479290.8
8	6.283185	184332.62	106101	644536.9	413644.3

Each model displays an increase in shear and elastic moduli towards the outer curvature of the aorta, where there is the least growth. Figures 15 and 16 display the approximate relationship between angular position and the moduli, based on the average values:

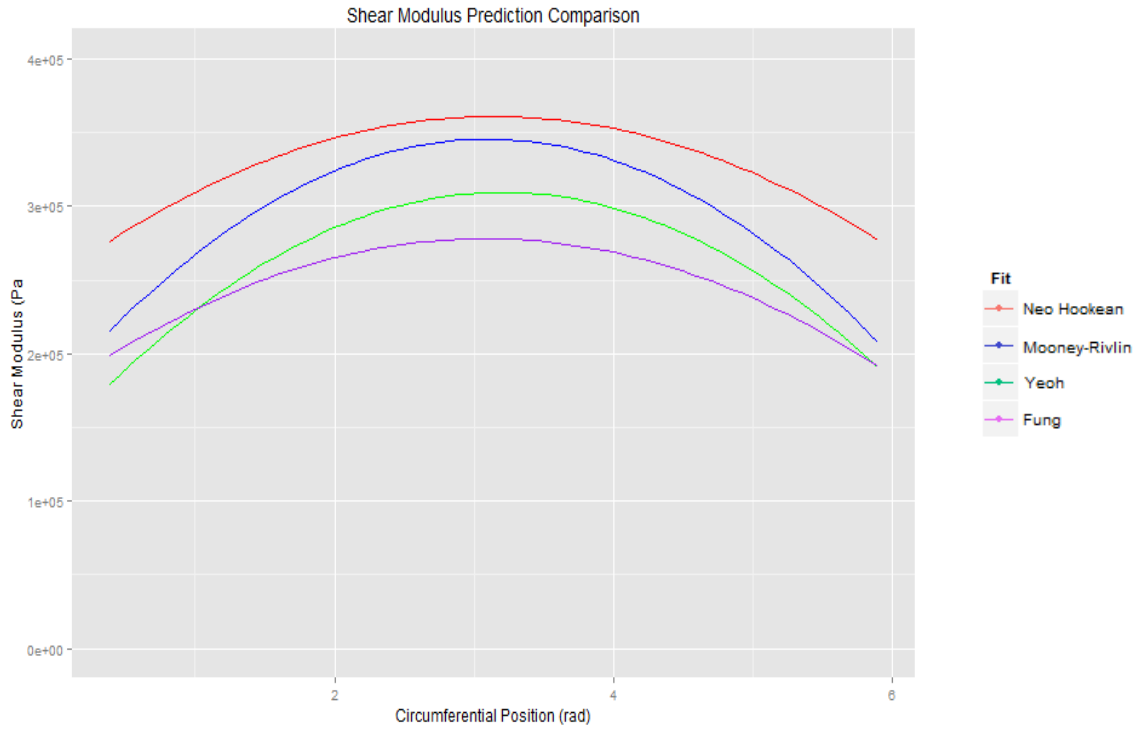


Figure 15: Prediction of shear modulus from models as a function of circumferential position at $\lambda = 1.4$

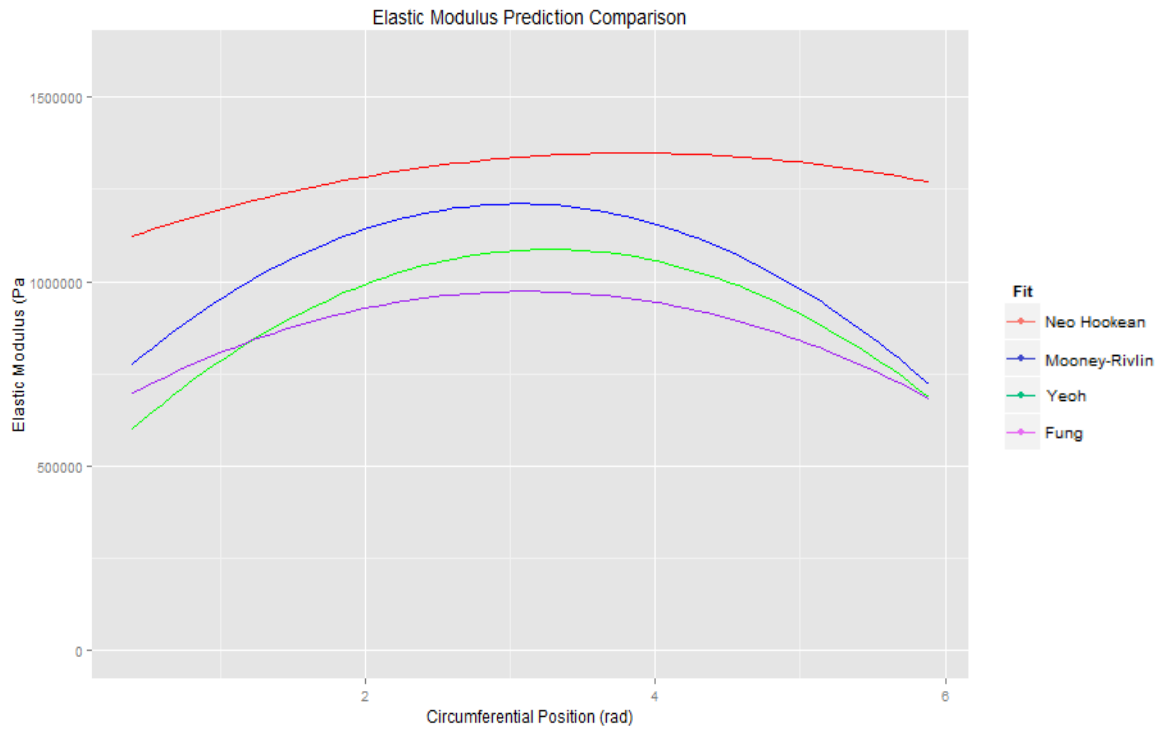


Figure 16: Prediction of elastic modulus from models as a function of circumferential position at $\lambda = 1.4$

All models show a reasonable relationship between the radial position and shear modulus. The average difference between the shear modulus of the inner and outer curvature is approximately 0.1 MPa, roughly a 35% decrease. This corresponds to a 30% increase in the average wall thickness.

The relative error between the models and data was calculated at strain intervals of 10%... The average results across all tests are shown in Figure 17.

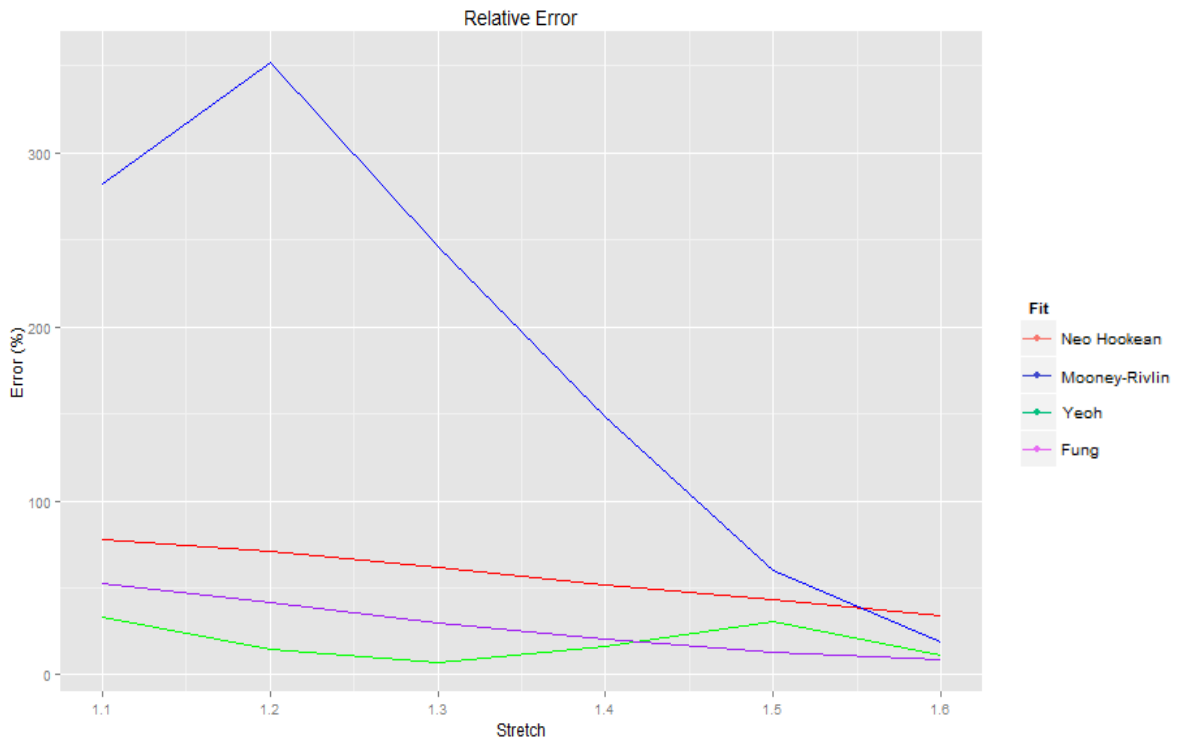


Figure 17: Average relative error of models at different stretch rates

The Mooney-Rivlin model starts off inaccurate, especially with the smaller values. All models show a trend towards lower relative error as the strain gets larger. However, the Neo-Hookean model would become more inaccurate past this limit as a result of its static shear modulus

5.2 Circumferential Testing

Only one test was deemed viable for strain tracking, with the others either having too poor video resolution or an insufficient amount of contrast in the staining pattern. The resulting video, mesh, and strain are displayed in Figure 18

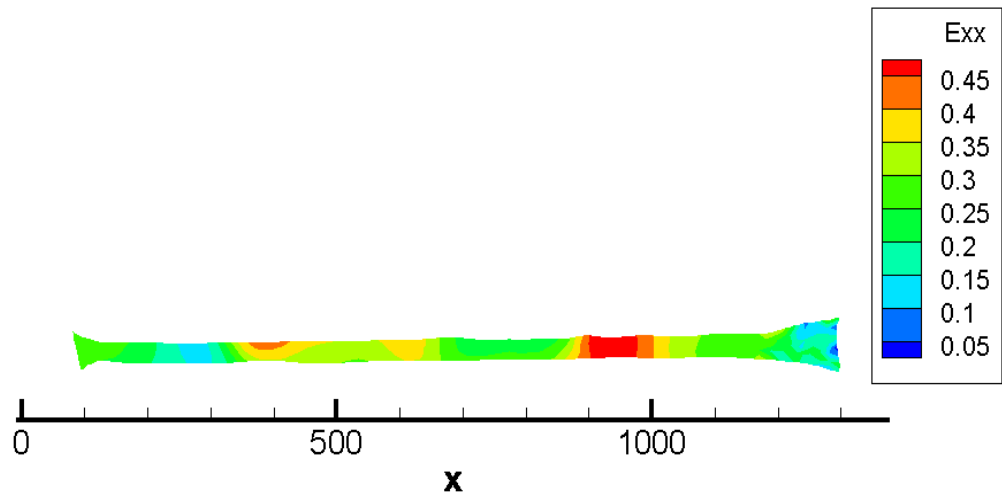


Figure 18: Video capture, meshing, and strain results of circumferential strain tracking

Using the strained cross-sectional area, it is possible to predict an elastic modulus along the length of the specimen. The strain and elastic modulus are shown in Figure 19.

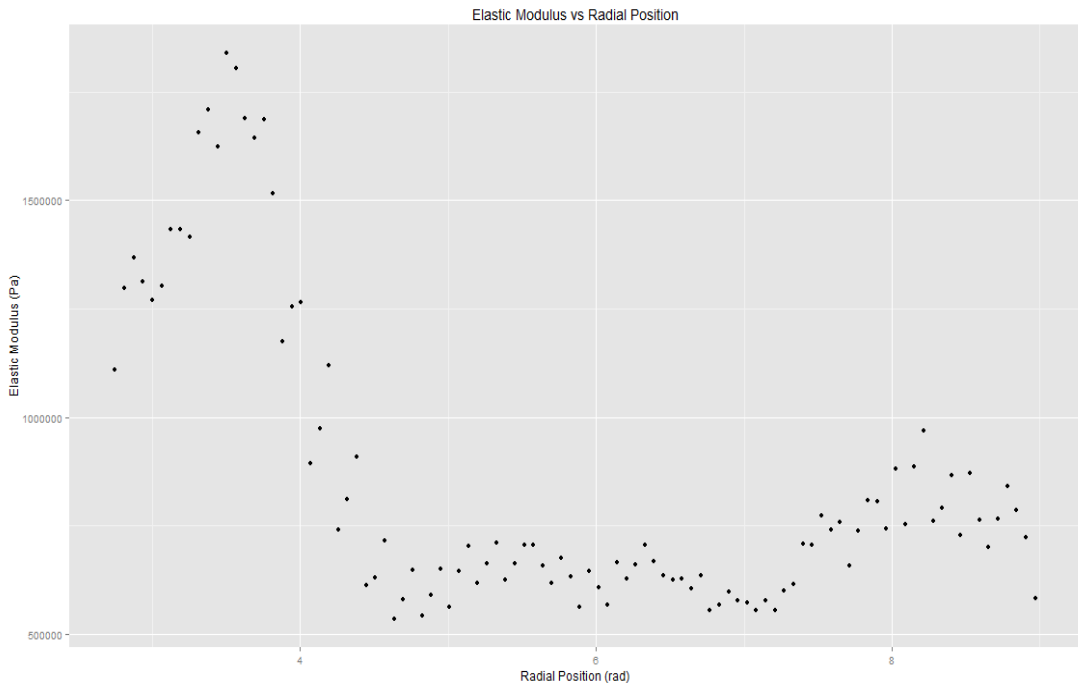
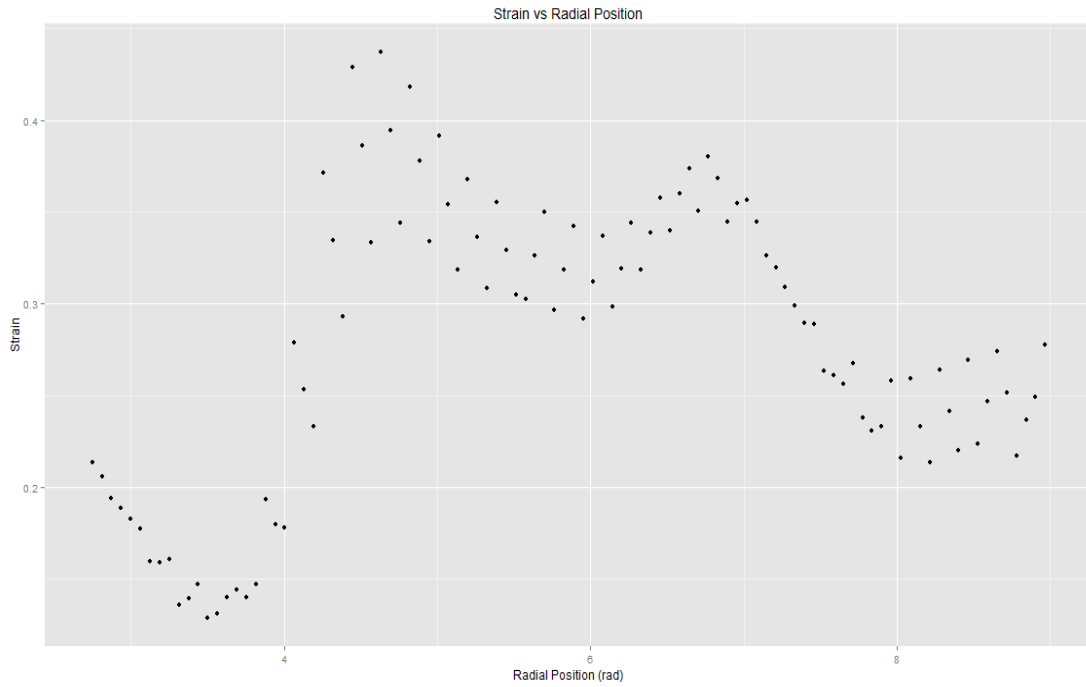


Figure 19: A) Strain vs circumferential position. B) Elastic Modulus vs circumferential position

The modulus displays the same behavior as during uniaxial tests, increasing in sections with less wall growth. It should be noted that this test was only to demonstrate the material behavior. A large sample size would be required to determine mechanical properties with any accuracy.

5.3 Contractile Testing

Every aortic half-ring that was studied elicited a definite contraction when treated with the norepinephrine solution. The results are displayed in Table 9

Table 10: Contractile Test Results

		1	2	3	4	5	6	7	8
	Thickness (mm)	2.79	2.54	2.39	2.34	3.23	3.00	2.66	2.48
1st	Initial Force (g)	2.041	2.033	1.979	2.134	2.247	2.300	2.211	2.095
Cycle	Final Force (g)	2.370	2.124	2.304	2.461	2.459	2.751	3.203	2.639
	change (g)	0.329	0.091	0.325	0.327	0.212	0.451	0.992	0.544
	g/mm	0.117	0.035	0.135	0.139	0.065	0.150	0.372	0.219
2nd	Initial Force (g)	1.296	1.955	1.990	2.171	2.131	2.109	3.186	2.031
Cycle	Final Force (g)	1.498	2.404	2.239	2.487	2.213	2.353	4.127	2.303
	change (g)	0.202	0.449	0.249	0.316	0.082	0.244	0.941	0.272

g/mm	0.072	0.176	0.104	0.135	0.025	0.081	0.353	0.109
------	-------	-------	-------	-------	-------	-------	-------	-------

It was observed that the prepared specimen halves from the inner aortic curvature elicited much stronger reactions; reaching an average peak contractile force of 25% above that of the resting forces. In contrast, the outer halves elicited peaks at 13% above their control forces. When taking the variable thicknesses into account, the outer halves contracted twice as much as the inner halves per millimeter of wall thickness. All samples elicited a decreased reaction during subsequent cycles of buffers. On the second cycle, both halves performed comparably (.12 and .14 g/mm for the outer and inner halves, respectively).

Conclusions & Future Considerations

The hyperelastic models employed in my thesis fit very well, as the tissue displays characteristic strain stiffening until the avulsion force is reached. The primary results demonstrate the mechanical behaviors of the artery wall will correlate as a function of its radial position, as well as its changes associated with aortic aneurysm growth. The inner portion of the aortic arch curvature, which elicited thicker walls, displayed a 35% lower shear modulus than the outer curvature, on average. This could be due to the growth of the media specifically, with recruitment of elastin fibers. This may help the vessel regulate its deformation during physiological function, ensuring the walls expand and contract a similar amount.

The circumferential test displayed the same general trend as the axial tests, with the modulus of elasticity decreasing as the wall thickness increased. It should be noted that due to the earlier described difficulties in recording the reproducible tests and time constraints, more studies were not able to be performed and analyzed. However, future experiments by others could determine how anisotropy and fiber direction is affected by the asymmetric growth of the arch.

The contractile investigations showed increased vasoconstriction response to the norepinephrine buffer as a result of increasing wall thickness due to growth. This suggests the recruitment of additional smooth muscle cells, which supports the theory of the tunica media experiencing growth. Further testing could be done at different concentrations of norepinephrine to determine the change more accurately.

While this study gives an insight into the elastic properties, it does not address the effects of growth on viscoelastic behavior. It would be beneficial to examine this in depth, as well as experimentally determine the physiological makeup. Methods such as mass

spectrometry would give more certain results than drawing conclusions from force-response behavior.

Bibliography

1. Fawcett D. *A Textbook of Histology*. 10th ed. W. B. Saunders; 1975.
2. Gray H. *Anatomy of the Human Body*. Philadelphia: Lea and Febiger; 1918.
3. Ren H, Hakki A, Kotler MN, Iskandrian AS. Exercise Systolic Blood Pressure : A Powerful Determinant of Increased Left Ventricular Mass in Patients With Hypertension. 1985;5(5):1224-1231. doi:10.1016/S0735-1097(85)80029-2.
4. American Heart Association. Understanding Blood Pressure Readings. National Health Council. doi:10.1161/CIR.0b013e31828124ad.
5. Alford PW, Taber LA. Computational study of growth and remodelling in the aortic arch. *Comput Methods Biomech Biomed Engin*. 2008;11(5):525-538. doi:10.1080/10255840801930710.
6. National Heart Lung and Blood Institute. Atherosclerosis-Related Disease. <http://www.nhlbi.nih.gov/health/health-topics/topics/atherosclerosis>. Published 2015. Accessed December 14, 2015.
7. Sheet S. TCD Series Digital Force Testers. 2010;(February).
8. Olympus. *Olympus Digital Camera E-PL3 Instruction Manual*. Vol 18.; 1999.
9. Grass Products. Force Displacement Transducer - Model FT03. <http://www.grasstechnologies.com/products/transducers/ft03.html>. Published 2016. Accessed February 2, 2016.
10. OWNER'S MANUAL FOR EPILOG Fusion -MODEL 13000 Contents at a Glance. 2013. www.epiloglaser.com/service.htm.
11. Mihai LA, Chin L, Janmey PA, Goriely A. A comparison of hyperelastic constitutive models applicable to brain and fat tissues. doi:10.1098/rsif.2015.0486.

Appendix A: Matlab Code

Avulsion Force Determination

```
%Ross Hinrichsen
%Visible Heart Lab
%12/16/15

%This script allows graphical selection of the first breakage point to
%set the range for later analysis. It also outputs the absolute maximum
%force.

clear all
close all

%Point the script at the tsv files

location = 'C:/Users/Ross/Documents/Thesis/Tests/Arch Tests/';
location = [location, 'All/'];
files = dir(location)
files = files(3:length(files));

for i=1:length(files);

    filename = files(i).name;
    locfile = [location, filename];
    data = importdata(locfile);

    max_f(i) = -min(data.data(:,3));

    figure(i);
    plot(data.data(:,1),-1 * data.data(:,3));
    title(filename)

    [bin(i),F(i)] = ginput(1); %Pick the first point of failure

end

bin = transpose(bin);
bin = round(bin);

close all
```


Neo-Hookean Curve Fitting

```
%Ross Hinrichsen
%Visible Heart Lab
%12/16/15

%The purpose of this program is to take experimental data from the
uniaxial
%pull tester, specify the region before breakage, and fit the data to
%hyperelastic solid models: Neo-Hookean, Fung, Mooney-Rivlin, Yeoh,

tic

clear all
close all

%Point the script at the tsv files

location = 'C:/Users/Ross/Documents/Thesis/Tests/Arch Tests/';
location = [location, 'All/'];
files = dir(location);
files = files(3:length(files));

%Grab the dimensions of each test from the spreadsheet

w = xlsread('C:/Users/Ross/Documents/Thesis/aorta.xlsx','Arch Pull
Tests #','G2:G157');
h = xlsread('C:/Users/Ross/Documents/Thesis/aorta.xlsx','Arch Pull
Tests #','H2:H157');
L = xlsread('C:/Users/Ross/Documents/Thesis/aorta.xlsx','Arch Pull
Tests #','I2:I157');
final = xlsread('C:/Users/Ross/Documents/Thesis/aorta.xlsx','Arch Pull
Tests #','K2:K157');

fo =
fitoptions('method','NonlinearLeastSquares','Robust','On','Algorithm','
Levenberg-Marquardt');

for i=1:length(files);

    filename = files(i).name;
    locfile = [location, filename];
    data = importdata(locfile);

    x = data.data(1:final(i),4) / L(i) + 1; % Lambda (dimensionless)
    a = w(i)*h(i); %original area
    A = a*x.^-1; %Area during stretch
    s = -
0.5*data.data(1:final(i),3)./A.*data.data(1:final(i),4)./L(i)*1000000;
%strain energy
```

```

fo =
fitoptions('method','NonlinearLeastSquares','Robust','On','Algorithm','
Levenberg-Marquardt');
ok = isfinite(x) & isfinite(s);

%Neo Hookian
st_NH = 0.05;
set(fo,'Startpoint',st_NH);
ft_NH = fittype('u*0.5*(x^2+2/x-3)',...
'dependent',{'y'},'independent',{'x'},...
'coefficients',{'u'});

[NH,nhgof] = fit(x(ok),s(ok),ft_NH,fo);
NeoHook(i,:) = [NH.u nhgof.rsquare];

%Find relative error at different stretch factors

%      u = [s(find(x>1.0999,1)), s(find(x>1.1999,1)),
s(find(x>1.2999,1)), s(find(x>1.3999,1)), s(find(x>1.4999,1)),
s(find(x>1.5999,1))];
%      if length(u) == 3;
%          u = [u 0 0 0];
%      elseif length(u) == 4;
%          u = [u 0 0];
%      elseif length(u) == 5;
%          u = [u 0];
%      end;
%
%      v = [NH.u*0.5*(1.1^2+2/1.1-3),NH.u*0.5*(1.2^2+2/1.2-
3),NH.u*0.5*(1.3^2+2/1.3-3),...
%          NH.u*0.5*(1.4^2+2/1.4-3),NH.u*0.5*(1.5^2+2/1.5-
3),NH.u*0.5*(1.6^2+2/1.6-3)];
%
%
%      error(i,:) = abs(1-u.*v.^-1);

end

clear A L NH a data filename files final fo ft_NH h i location locfile
nhgof ok s st_NH u v w x

toc

close all

```

Mooney-Rivlin Curve Fitting

```
%Ross Hinrichsen
%Visible Heart Lab
%12/16/15

%The purpose of this program is to take experimental data from the
uniaxial
%pull tester, specify the region before breakage, and fit the data to
%hyperelastic solid models

tic

clear all
close all

%Point the script at the tsv files

location = 'C:/Users/Ross/Documents/Thesis/Tests/Arch Tests/';
location = [location, 'All/'];
files = dir(location);
files = files(3:length(files));

%Grab the dimensions of each test from the spreadsheet

w = xlsread('C:/Users/Ross/Documents/Thesis/aorta.xlsx', 'Arch Pull
Tests #', 'G2:G157');
h = xlsread('C:/Users/Ross/Documents/Thesis/aorta.xlsx', 'Arch Pull
Tests #', 'H2:H157');
L = xlsread('C:/Users/Ross/Documents/Thesis/aorta.xlsx', 'Arch Pull
Tests #', 'I2:I157');
final = xlsread('C:/Users/Ross/Documents/Thesis/aorta.xlsx', 'Arch Pull
Tests #', 'K2:K157');

for i=1:length(files);

    filename = files(i).name;
    locfile = [location, filename];
    data = importdata(locfile);

    x = data.data(1:final(i),4) / L(i) + 1; % Lambda (dimensionless)
    a = w(i)*h(i); %original area
    A = a*x.^-1; %Area during stretch
    s = -
    0.5*data.data(1:final(i),3) ./A.*data.data(1:final(i),4) ./L(i)*1000000;
    %strain energy
```

```

fo =
fitoptions('method','NonlinearLeastSquares','Robust','On','Algorithm','
Levenberg-Marquardt');
ok = isfinite(x) & isfinite(s);

%Mooney Rivlin
st_MR = [0.997, 1];
set(fo,'Startpoint',st_MR);
ft_MR = fittype('a*0.5*(x^2+2/x-3)+b*0.5*(2*x+1/(x^2)-3)',...
'dependent',{'y'},'independent',{'x'},...
'coefficients',{'a','b'});

[MR, mrgof] = fit(x(ok),s(ok),ft_MR,fo);
Coeffs(i,:) = [MR.a MR.b mrgof.rsquare];

u = [s(find(x>1.0999,1)), s(find(x>1.1999,1)), s(find(x>1.2999,1)),
s(find(x>1.3999,1)), s(find(x>1.4999,1)), s(find(x>1.5999,1))];
if length(u) == 3;
    u = [u 0 0 0];
elseif length(u) == 4;
    u = [u 0 0];
elseif length(u) == 5;
    u = [u 0];
end;

v = [MR.a*0.5*(1.1^2+2/1.1-3)+MR.b*0.5*(2*1.1+1/(1.1^2)-
3),MR.a*0.5*(1.2^2+2/1.2-3)+MR.b*0.5*(2*1.2+1/(1.2^2)-3),...
MR.a*0.5*(1.3^2+2/1.3-3)+MR.b*0.5*(2*1.3+1/(1.3^2)-
3),MR.a*0.5*(1.4^2+2/1.4-3)+MR.b*0.5*(2*1.4+1/(1.4^2)-3)...
MR.a*0.5*(1.5^2+2/1.5-3)+MR.b*0.5*(2*1.5+1/(1.5^2)-
3),MR.a*0.5*(1.6^2+2/1.6-3)+MR.b*0.5*(2*1.6+1/(1.6^2)-3)];

error(i,:) = abs(1-u.*v.^-1);

end

clear A L MR a data filename files final fo ft_MR h i location locfile
mrgof ok s st_MR u v w x
toc

close all

```

Yeoh Curve Fitting

```
%Ross Hinrichsen
%Visible Heart Lab
%12/16/15

%The purpose of this program is to take experimental data from the
uniaxial
%pull tester, specify the region before breakage, and fit the data to
%hyperelastic solid models

tic

clear all
close all

%Point the script at the tsv files

location = 'C:/Users/Ross/Documents/Thesis/Tests/Arch Tests/';
location = [location, 'All/'];
files = dir(location);
files = files(3:length(files));

%Grab the dimensions of each test from the spreadsheet

w = xlsread('C:/Users/Ross/Documents/Thesis/aorta.xlsx','Arch Pull
Tests #','G2:G157');
h = xlsread('C:/Users/Ross/Documents/Thesis/aorta.xlsx','Arch Pull
Tests #','H2:H157');
L = xlsread('C:/Users/Ross/Documents/Thesis/aorta.xlsx','Arch Pull
Tests #','I2:I157');
final = xlsread('C:/Users/Ross/Documents/Thesis/aorta.xlsx','Arch Pull
Tests #','K2:K157');

for i=1:length(files);

    filename = files(i).name;
    locfile = [location, filename];
    data = importdata(locfile);

    x = data.data(1:final(i),4) / L(i) + 1; % Lambda (dimensionless)
    a = w(i)*h(i); %original area
    A = a*x.^-1; %Area during stretch
    s = -
    0.5*data.data(1:final(i),3)./A.*data.data(1:final(i),4)./L(i)*1000000;
    %strain energy

    fo =
    fitoptions('method','NonlinearLeastSquares','Robust','On','Algorithm','
    Levenberg-Marquardt');
    ok = isfinite(x) & isfinite(s);
```

```

% Yeoh
st_Y = [0 0 0];
set(fo, 'Startpoint', st_Y);
ft_Y = fittype('a*(x^2+2/x-3)+b*(x^2+2/x-3)^2+c*(x^2+2/x-3)^3', ...
'dependent', {'y'}, 'independent', {'x'}, ...
'coefficients', {'a', 'b', 'c'});

[Y, ygof] = fit(x(ok), s(ok), ft_Y, fo);
Ye(i, :) = [Y.a Y.b Y.c ygof.rsquare];

u = [s(find(x>1.0999,1)), s(find(x>1.1999,1)), s(find(x>1.2999,1)),
s(find(x>1.3999,1)), s(find(x>1.4999,1)), s(find(x>1.5999,1))];
if length(u) == 3;
    u = [u 0 0 0];
elseif length(u) == 4;
    u = [u 0 0];
elseif length(u) == 5;
    u = [u 0];
end;

v = [Y.a*(1.1^2+2/1.1-3)+Y.b*(1.1^2+2/1.1-3)^2+Y.c*(1.1^2+2/1.1-
3)^3, ...
Y.a*(1.2^2+2/1.2-3)+Y.b*(1.2^2+2/1.2-3)^2+Y.c*(1.2^2+2/1.2-
3)^3, ...
Y.a*(1.3^2+2/1.3-3)+Y.b*(1.3^2+2/1.3-3)^2+Y.c*(1.3^2+2/1.3-
3)^3, ...
Y.a*(1.4^2+2/1.4-3)+Y.b*(1.4^2+2/1.4-3)^2+Y.c*(1.3^2+2/1.4-
3)^3, ...
Y.a*(1.5^2+2/1.5-3)+Y.b*(1.5^2+2/1.5-3)^2+Y.c*(1.3^2+2/1.5-
3)^3, ...
Y.a*(1.6^2+2/1.6-3)+Y.b*(1.6^2+2/1.6-3)^2+Y.c*(1.6^2+2/1.6-
3)^3];

error(i, :) = abs(1-u.*v.^-1);

end

clear A L Y a data filename files final fo ft_Y h i location locfile
ygof ok s st_Y u v w x

toc

close all

```

Fung Curve Fitting

```
%Ross Hinrichsen
%Visible Heart Lab
%12/16/15

%The purpose of this program is to take experimental data from the
uniaxial
%pull tester, specify the region before breakage, and fit the data to
%hyperelastic solid models

tic

clear all
close all

%Point the script at the tsv files

location = 'C:/Users/Ross/Documents/Thesis/Tests/Arch Tests/';
location = [location, 'All/'];
files = dir(location);
files = files(3:length(files));

%Grab the dimensions of each test from the spreadsheet

w = xlsread('C:/Users/Ross/Documents/Thesis/aorta.xlsx','Arch Pull
Tests #','G2:G157');
h = xlsread('C:/Users/Ross/Documents/Thesis/aorta.xlsx','Arch Pull
Tests #','H2:H157');
L = xlsread('C:/Users/Ross/Documents/Thesis/aorta.xlsx','Arch Pull
Tests #','I2:I157');
final = xlsread('C:/Users/Ross/Documents/Thesis/aorta.xlsx','Arch Pull
Tests #','K2:K157');

for i=1:length(files);

    filename = files(i).name;
    locfile = [location, filename];
    data = importdata(locfile);

    x = data.data(1:final(i),4) / L(i) + 1; % Lambda (dimensionless)
    a = w(i)*h(i); %original area
    A = a*x.^-1; %Area during stretch
    s = -
0.5*data.data(1:final(i),3) ./A.*data.data(1:final(i),4) ./L(i)*1000000;
%strain energy
```

```

fo =
fitoptions('method','NonlinearLeastSquares','Robust','On','Algorithm','
Levenberg-Marquardt','MaxIter',100000);
ok = isfinite(x) & isfinite(s);

    %Fung
st_F = [0.1 100000];
set(fo,'Startpoint',st_F);
ft_F = fitype('C*(a*(x^2+2/x-3)+exp(a*(x^2+2/x-3))-1)/(2*a)',...
'dependent',{'y'},'independent',{'x'},...
'coefficients',{'a','C'});

[F,fgof] = fit(x(ok),s(ok),ft_F,fo);
Coeffs(i,:) = [F.C F.a fgof.rsquare];

u = [s(find(x>1.0999,1)), s(find(x>1.1999,1)), s(find(x>1.2999,1)),
s(find(x>1.3999,1)), s(find(x>1.4999,1)), s(find(x>1.5999,1))];
if length(u) == 3;
    u = [u 0 0 0];
elseif length(u) == 4;
    u = [u 0 0];
elseif length(u) == 5;
    u = [u 0];
end;

v = [F.C*(F.a*(1.1^2+2/1.1-3)+exp(F.a*(1.1^2+2/1.1-3))-
1)/(2*F.a),F.C*(F.a*(1.2^2+2/1.2-3)+exp(F.a*(1.2^2+2/1.2-3))-
1)/(2*F.a),...
F.C*(F.a*(1.3^2+2/1.3-3)+exp(F.a*(1.3^2+2/1.3-3))-
1)/(2*F.a),F.C*(F.a*(1.4^2+2/1.4-3)+exp(F.a*(1.4^2+2/1.4-3))-
1)/(2*F.a),...
F.C*(F.a*(1.5^2+2/1.5-3)+exp(F.a*(1.5^2+2/1.5-3))-
1)/(2*F.a),F.C*(F.a*(1.6^2+2/1.6-3)+exp(F.a*(1.6^2+2/1.6-3))-
1)/(2*F.a)];

error(i,:) = abs(1-u.*v.^-1);

end

clear A L F a data filename files final fo ft_F h i location locfile
fgof ok s st_F u v w x
toc

close all

```


Strain Tracking Stretched Width Analysis

```
close all
clear all
location = 'C:/Users/Ross/Documents/Thesis/';
location = [location, 'Strain Tracking Results/'];
files = dir(location);
I = imread('C:/Users/Ross/Documents/Thesis/Strain Tracking
Results/result10_crop.png');
image(I)

xbegin=round(ginput(1));
xend=round(ginput(1));

step = 6; % how many pix per step
len = (xend(1)-xbegin(1))/step; % number of tested points
X = xbegin(1);

for i = 1:len
    Y = 700;
    RGB = impixel(I,X,Y);
    while RGB == [255,255,255];
        Y = Y +1;
        RGB = impixel(I,X,Y);
    end
    T(i) = Y;
    sum = 760;

    while sum ~= 765;
        Y = Y + 1
        RGB = impixel(I,X,Y);
        sum = RGB(1) + RGB(2) + RGB(3);
    end
    B(i) = Y;
    X = X + 6;

end

con = (xend(1)-xbegin(1))/90; %pix/mm

Diff = transpose(B - T); %pix

Height = Diff/con;
```